8th European Congress on Computational Methods in Applied Sciences and Engineering (ECCOMA2022)
June 5-9, 2022, Oslo, Norway

Dynamic Response of Offshore Monopile Wind Turbine under Nonlinear Irregular Ocean Waves

HADI PEZESHKI*, DIMITRIOS PAVLOU†
AND SUDATH C. SIRIWARDANE †

*University of Stavanger
Hadi.Pezeshki@uis.no

† University of Stavanger
dimitrios.g.pavlou@uis.no

† University of Stavanger
sasc.siriwardane@uis.no

Keywords: Offshore Wind Turbine, Response, Soil-Structure Interactions, Wave-Structure interactions, second-order nonlinear ocean waves, stress history.

ABSTRACT

Offshore wind turbines (OWT) are exposed to different categories of ocean waves during their lifetime. Most ocean waves are categorized in the second-order nonlinear theory in normal and severe sea states, and their spectra combine different heights and frequencies. In the present study, a model for the dynamic response of OWTs to the wave load obtained irregular second-order nonlinear ocean waves is proposed. The foundation-wave-structure interaction and the effect of the nacelle-rotor assembly are simulated. Numerical results are provided and discussed.

1. Introduction

Offshore structures are exposed to harsh, unpredictable, but random ocean environmental loading. These loads are consistently applied to these structures, increasing the risk of fatigue accumulation damage. This is the most crucial cause of the failures reported in the past years, accounting for 25% of total damages [1]. Moreover, almost half of the operating OWTs in Europe will reach their design life by the end of 2030 [2]. An accurate estimation of fatigue accumulated damage is therefore not only useful for design, but also for estimating the remaining life of operating structures.

The main input for investigating fatigue accumulation damage is the stress history of the hotspots of the structure [3]. It is possible to obtain these data either by measuring the stress at some points of the operating structures or by generating them from mathematical models. Measuring field data, apart from accessibility and expenses, is sometimes impossible for inaccessible locations such as monopile under the seabed. Despite its value, it provides only a local assessment of the history of stress that may miss some other critical hotspots. Besides, utilizing field data in fatigue life analysis requires signal processing [4,5] and data management techniques [6]. An alternative method is to generate data via mathematical models by considering different properties of the structure.

The mathematical models can be established either by discretizing the structure into small elements through finite element methods [7] or by considering it as a continuous function via partial differential equations [8,9]. Modeling the OWT by finite element methods has been the most popular method among researchers in recent years [10–12]. Banerjee et al. [13] established a model by discretizing the continuous mass into lumped masses and creating a multi-degree of freedom model to analyze the structure under random wind and wave load. Alkhoury et al. [14] used a commercial finite element package, Abaqus/Standard, to provide a fully detailed model. Some other researchers have used software programs developed explicitly in the case of OWTs, such as FAST, HAWC2, BLADED, etc. However, dynamic analysis of OWTs as a continuous system is rare. Wang et al. [15] modeled an onshore wind turbine using the thin-walled beam theory. Povlou [9] has solved the partial deferential equation governing the motion of the OWT's monopile by using the integral transformation.

With increasing water depth, wave loads contribute significantly to the dynamic response of OWTs [16]. Moreover, recently, researchers have reported the complexity of ocean wave simulations and their application to dynamic analysis. For instance, Natarjan [17] implemented second-order wave theory to investigate the impact of these nonlinear wave models on the design load of OWT's monopile. Yingguang Wang [18] aimed to implement irregular nonlinear waves into the dynamic response by a linear transform method.

This study aims to develop a model to generate the stress history required for the fatigue analysis of OWT's structures. The objective is to obtain the dynamic response as a single function with the input of the parameters of the irregular second-order waves utilized in Morison's formula [19]. The OWT monopile is considered a continuous system, and equations of motion are formed using the Euler-Bernoulli beam theory.

2. Methodology

A bottom-fixed monopile-supported OWT is addressed in this paper. The typical form of these structures is shown in Figure 1-a. This structure is modeled as two sections, the tower and the monopile, separated at the platform level. The monopile is also separated from the sea level, monopile underwater and above water, Figure 1-b. Also included in Table 1 are definitions of the symbols used in this paper.

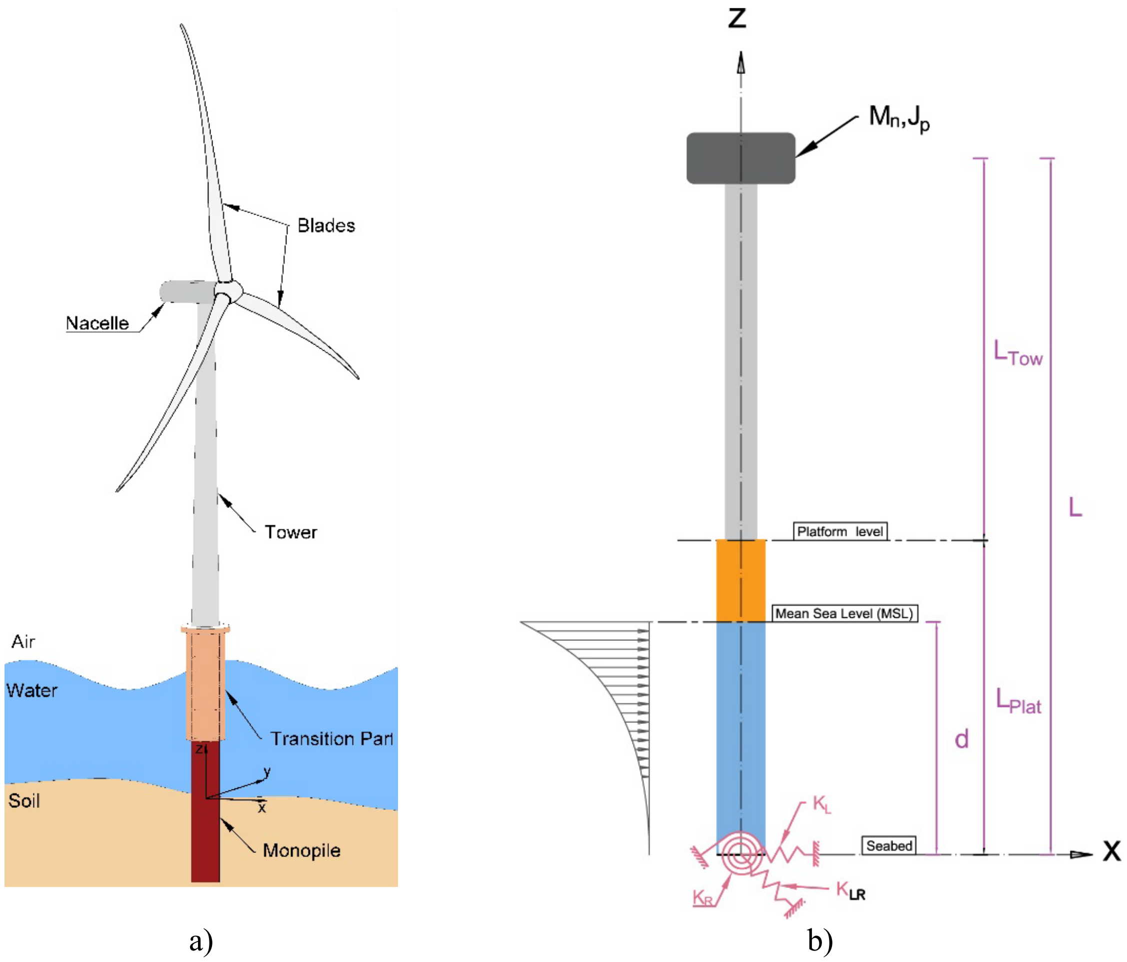

Figure 1: a) The typical bottom-fixed monopile supported OWT, b) The defined model

Table 1) Symbols definition

Symbol	Structural properties
L	Nacelle level from the seabed (m)
$x_{Tow}(z,t)$	The motion of the tower
$x_{MA}(z,t)$	The motion of the monopile above water
$x_{MU}(z,t)$	The motion of the monopile underwater
L_{Tow}	Tower length (m)
D_{Tow}	Tower average diameter (m)
t_{Tow}	Tower average thickness (m)
m_{Tow}	Tower mass of unit length (Kg/m)
E_{Tow}	Tower Young's modulus (GPa)
EI_{Tow}	Flexural rigidity of the tower, i.e., $E_{Tow}I_{Tow}$ ($GPa.m^4$)
M_n	Nacelle-Rotor assembly mass (Kg)
J_p	Nacelle-Rotor assembly rotational inertia ($Kg.m^2$)
L_{Plat}	Platform level from the seabed (m)
D_{Mon}	Monopile average diameter (m)
t_{Mon}	Monopile average thickness (m)
A_{Mon}	Monopile cross-sectional area (m^2)
m_{Mon}	Monopile mass of unit length (Kg/m)
E_{Mon}	Monopile Young's modulus (GPa)
EI_{Mon}	Flexural rigidity of the monopile, i.e., $E_{Mon}I_{Mon}$ ($GPa.m^4$)
ρ_s	Material Density (Kg/m^3)
Symbol	**Support Stiffness**
K_L	Lateral stiffness (GN/m)
K_{LR}	Cross stiffness (GN)
K_R	Rotational stiffness ($GN.m$)
Symbol	**Hydrodynamic loading properties**
d	Water depth (m)
C_D	Drag coefficient
C_A	Added mass coefficient
C_M	Inertia coefficient
ρ_w	Sea water density (Kg/m^3)
λ	Ocean wavelength (m)
k	Ocean wavenumber (m^{-1})
H	Ocean wave height (m)
g	Gravitational acceleration (m/s^2)

2.1. Formulation of the equations of motion

As mentioned earlier, the structure of the OWT is modeled in three sections. Using the Euler-Bernoulli beam theory, the corresponding equations of motion are

$$x_{Tow}^{(iv)}(z,t) + \frac{1}{a_{Tow}^2}\ \ddot{x}_{Tow}(z,t)\ = 0\,, \qquad for\ L_{Plat} \le z \le L \tag{1}$$

$$x_{MA}^{(iv)}(z,t) + \frac{1}{a_{MA}^2}\ \ddot{x}_{MA}(z,t)\ = 0\,, \qquad for\ d < z \le L_{Plat} \tag{2}$$

$$x_{MU}^{(iv)}(z,t) + \frac{1}{a_{MU}^2}\ \ddot{x}_{MU}(z,t)\ = \frac{1}{EI_{Mon}} Q(z,t), \qquad for\ 0 < z \le d \tag{3}$$

Where

$$a_{\mathrm{Tow}}^2 = \frac{EI_{Tow}}{m_{Tow}} \tag{4}$$

$$a_{\mathrm{MA}}^2 = \frac{EI_{Mon}}{m_{Mon}} \tag{5}$$

$$a_{\mathrm{MU}}^2 = \frac{EI_{Mon}}{m_{Mon} + \rho_w C_A A_{Mon}} \tag{6}$$

$$Q(z,t) = \rho_w C_M A_{Mon} \dot{u}(z,t) + \frac{1}{2}\rho_w C_D D_{Mon} u(z,t)|u(z,t)| \tag{7}$$

The added mass term, $\rho_w C_A A_{Mon}$, is included in Eq. (3), which is the equation of motion of the underwater part of the monopile. The equations of motion in Eqs. (1) to (3) are regulated by four boundary conditions. Two of them are at the structure's top and bottom, representing the presence of the nacelle-rotor assembly mass and rotational mass of inertia and soil-structure interactions defined by the coupled springs, respectively. They are

$$-EI_{Mon}\, x_{MU}'''(0,t) = \mathrm{K}_L x_{MU}(0,t) + K_{LR} x_{MU}'(0,t) \tag{8}$$

$$EI_{Mon}\, x_{MU}''(0,t) = K_{LR} x_{MU}(0,t) + \mathrm{K_R}\, x_{MU}'(0,t) \tag{9}$$

And

$$-EI_{Tow}\, x_{Tow}''(L,t) = J_P \ddot{x}_{Tow}'(L,t) \tag{10}$$

$$EI_{Tow}\, x_{Tow}'''(L,t) = M_N \ddot{x}_{Tow}(L,t) \tag{11}$$

The other two sets of boundary conditions are at the platform level, where the cross-sectional discrepancy exists between the monopile and the tower, and the sea level, where the monopile is separated for underwater, where the added mass is included, and above water. They are

$$x_{MA}(L_{Plat}, t) = x_{Tow}(L_{Plat}, t) \tag{12}$$

$$x'_{MA}(L_{Plat}, t) = x'_{Tow}(L_{Plat}, t) \tag{13}$$

$$EI_{Mon}x''_{MA}(L_{Plat}, t) = EI_{Tow}x''_{Tow}(L_{Plat}, t) \tag{14}$$

$$EI_{Mon}x'''_{MA}(L_{Plat}, t) = EI_{Tow}x'''_{Tow}(L_{Plat}, t) \tag{15}$$

And

$$x_{MU}(d, t) = x_{MA}(d, t) \tag{16}$$

$$x'_{MU}(d, t) = x'_{MA}(d, t) \tag{17}$$

$$x''_{MU}(d, t) = x''_{MA}(d, t) \tag{18}$$

$$x'''_{MU}(d, t) = x'''_{MA}(d, t) \tag{19}$$

Expansion in the natural modes is the method selected to solve the equations of motion. Several methods are proposed to solve these partial differential equations in the classical references [20,21]. For instance, Graff [21] introduced five methods, including the Finite Fourier transform, expansion in the natural modes, Laplace Transform, the combination of the Laplace transform and expansion in natural modes, and the solution by natural modes. Reviewing these methods reveals that using the method of expansion in natural modes is an appropriate choice in finding the solution as a single function. Expansion of the solution in the natural mode shapes requires taking the following steps:

1. Find the natural frequency and the corresponding mode shapes of the structure
2. Find the natural mode shapes and normalize them
3. Expand the external load into the natural mode shapes
4. Find the solution as a summation of the response in every mode shapes

2.2. Finding the natural frequencies and corresponding mode shapes

Finding the natural mode shapes begins working with the homogenous form of the equations of motion in Eqs. (1) to (3). Considering the natural mode shapes in the form of $x_n(z, t) = X_n(z)\, e^{-i\omega_n t}$ and substituting into equation of motions, they result in

$$X^{iv}_{Tn}(z) - \beta^4_{Tn}X_{Tn}(z) = 0, \qquad for\ L_{Plat} \le z \le L \tag{20}$$

$$X^{iv}_{MAn}(z) - \beta^4_{MAn}X_{MAn}(z) = 0, \qquad for\ d < z \le L_{Plat} \tag{21}$$

$$X^{iv}_{MUn}(z) - \beta^4_{MUn}X_{MUn}(z) = 0, \qquad for\ 0 < z \le d \tag{22}$$

Where

$$\omega_n^2 = a_{Tow}^2\, \beta_{Tn}^4 = a_{MU}^2\, \beta_{MUn}^4 = a_{MA}^2\, \beta_{MAn}^4 \tag{23}$$

β_{Tn}, β_{MAn} and β_{MUn} are defined as wavenumbers of the motion for the tower and monopile above water and underwater, respectively.

The general form of the solution for Eqs. (20) to (22), which are the ordinary fourth-order differential equations, is

$$X(z) = A_1\ cos(\beta\, z) + \ A_2\, cosh(\beta\, z) + A_3\ sin(\beta\, z) + A_4\ sinh(\beta\, z) \tag{24}$$

Also, the solution of $x_n(z,t) = X_n(z)\, e^{-i\omega_n t}$ should be introduced into the boundary conditions in Eqs. (8) to (19) to arrange a set of equations in which the only unknown is ω_n. To find ω_n, one can arrange these equations in the form of matrixes such that

$$\boldsymbol{P} \times \boldsymbol{D} = 0, \qquad \boldsymbol{D} = \{U_1\ \ U_2\ \ U_3\ \ U_4\ \ A_1\ \ A_2\ A_3\ A_4\ T_1\ \ T_2\ T_3\ T_4\}^T \tag{25}$$

Where P is the matrix containing the trigonometrical and hyper trigonometrical functions, and D is a vector consisting of constant coefficients required for the general form of the solution in Eq. (24). Therefore, the first two steps of finding the response can be taken as

Step 1: Providing $Det(\boldsymbol{P}) = 0$ gives the frequency equation and solving it results in the natural frequencies of the system.

Step 2: After finding the natural frequencies, the natural mode shapes can be calculated by determining the coefficient vectors $\boldsymbol{D}$. These coefficients can be found by substituting every natural frequency found in step 1 into $\boldsymbol{P}$ and calculating the eigenvector corresponding to the eigenvalue zero. The natural mode shapes can also be normalized to satisfy the following equation

$$\int_0^L \left(\frac{1}{a_{Tow}^2} X_{Tn}^2(z) + \frac{1}{a_{\mathrm{MA}}^2} X_{MAn}^2(z) + \frac{1}{a_{MU}^2} X_{MUn}^2(z) \right) dz = 1 \tag{26}$$

2.3. Solution for equations of motion

The general solution for the equations of motion using the expansion in the natural mode shapes is in the form of

$$\mathrm{x}(z,t) = \sum_{n=1}^{\infty} X_n(z)\, T(t) \tag{27}$$

Where $X_n(z)$ is the natural mode shapes of the system, which depends on the boundary conditions and $T_n(t)$ is the temporal part of the solution, which can be obtained from the expansion of the external load in the natural mode shapes. Substituting this solution into the equations of motion in Eq. (1) to (3), $T_n(t)$ can be found by solving the following second-order ordinary differential equation.

$$\ddot{T}(t)+\omega_n^2\mathrm{T}(t)=\frac{1}{EI_M}\int_0^d Q(z,t)X_n(z)dz \tag{28}$$

Step 3: Expanding the external load into the natural mode shapes of the structure is performed in Eq. (28) by solving the integration on the right side of this equation. Solving this integration and the differential equation are quite flexible for complex external loading. It can be performed either numerically or analytically for every $Q(z,t)$.

2.4. Solution for the nonlinear second-order irregular waves

Generally, irregular ocean waves are described by an idealized linear Gaussian state, assuming a symmetrical crest-trough. However, the real sea state does not follow this symmetricity. By increasing the wave height or decreasing the wavelength, the wave's profile becomes steeper and higher at the crest and flatter and shallower at the trough. Therefore, the linear Gaussian wave is not valid for the waves with higher steepness. The irregular nonlinear sea wave surface elevation can be written as [22,23]:

$$\eta(t)=\eta_1(t)+\eta_2(t) \tag{29}$$

Where

$$\eta_1(t)=\sum_{k=1}^{N} H_k\cos(\omega_k\, t+\varphi_k) \tag{30}$$

$$\begin{aligned}\eta_2(t)=&\sum_{n=1}^{N}\sum_{m=1}^{N} H_mH_nB_{mn}^{(+)}\cos\big((\omega_m+\omega_n)\,t+(\varphi_m+\varphi_n)\big)\\&+\sum_{n=1}^{N}\sum_{m=1}^{N} H_mH_nB_{mn}^{(-)}\cos\big((\omega_m-\omega_n)\,t+(\varphi_m-\varphi_n)\big)\end{aligned} \tag{31}$$

Where H_k are the random wave amplitude which is

$$E[H_k^2]=2\,S(\omega_k)\Delta\omega_k \tag{32}$$

$S(\omega_k)$ is obtained from the wave spectrum and $\Delta\omega_k$ is the difference between successive frequencies. φ_k is the phase angle which is a random number in the range of $[0,2\,\pi]$. $B_{mn}^{(\pm)}$ are quadratic Surface elevation transfer functions. In deep water, they are

$$B_{mn}^{(+)}=\frac{1}{4g}(\omega_m^2+\omega_n^2) \tag{33}$$

$$B_{mn}^{(-)} = \frac{1}{4g}(\omega_m^2 - \omega_n^2) \tag{34}$$

The transfer functions for the general water depth are given by:

$$B_{mn}^{(+)} = \frac{1}{4g}\left[\frac{R_{mn}^{(+)} - (g^2 k_m k_n - \omega_m^2 \omega_n^2)}{\omega_m \omega_n} + (\omega_m^2 + \omega_n^2)\right] \tag{35}$$

$$B_{mn}^{(-)} = \frac{1}{4g}\left[\frac{R_{mn}^{(-)} - (g^2 k_m k_n + \omega_m^2 \omega_n^2)}{\omega_m \omega_n} + (\omega_m^2 + \omega_n^2)\right] \tag{36}$$

Where

$$R_{mn}^{(+)} = \frac{(\omega_m + \omega_n)\big(\omega_n(g^2 k_m^2 - \omega_m^4) + \omega_m(g^2 k_n - \omega_n^4)\big)}{(\omega_m + \omega_n)^2 - g(k_m + k_n)\tanh\big((k_m + k_n)d\big)} + \frac{2(\omega_m + \omega_n)^2(g^2 k_m k_n - \omega_m^2 \omega_n^2)}{(\omega_m + \omega_n)^2 - g(k_m + k_n)\tanh\big((k_m + k_n)d\big)} \tag{37}$$

$$R_{mn}^{(-)} = \frac{(\omega_m - \omega_n)\big(\omega_n(g^2 k_m^2 - \omega_m^4) - \omega_m(g^2 k_n - \omega_n^4)\big)}{(\omega_m - \omega_n)^2 - g|k_m - k_n|\tanh(|k_m - k_n|d)} + \frac{2(\omega_m - \omega_n)^2(g^2 k_m k_n + \omega_m^2 \omega_n^2)}{(\omega_m - \omega_n)^2 - g|k_m - k_n|\tanh(|k_m - k_n|d)} \tag{38}$$

The corresponding velocity potential can also be written as:

$$\Phi(t) = \Phi_1(t) + \Phi_2(t) \tag{39}$$

Where

$$\Phi_1(t) = \sum_{k=1}^{N} \frac{gH_k}{\omega_k} \frac{\cosh(k_k\, z)}{\cosh(k_k d)} \sin(\omega_k\, t + \varphi_k) \tag{40}$$

$$\begin{aligned}\Phi_2(t) &= \\ &\frac{1}{4}\sum_{n=1}^{N}\sum_{m=1}^{N} \frac{H_m}{\omega_m}\frac{H_n}{\omega_n}\frac{\cosh\big((k_m+k_n)\, z\big)}{\cosh\big((k_m+k_n)d\big)}\frac{R_{mn}^{(+)}}{(\omega_m+\omega_n)}\sin\big((\omega_m+\omega_n)\, t + (\varphi_m+\varphi_n)\big) \\ &+\frac{1}{4}\sum_{n=1}^{N}\sum_{m=1}^{N} \frac{H_m}{\omega_m}\frac{H_n}{\omega_n}\frac{\cosh((k_m-k_n)\, z)}{\cosh((k_m-k_n)d)}\frac{R_{mn}^{(-)}}{(\omega_m-\omega_n)}\sin\big((\omega_m-\omega_n)\, t + (\varphi_m-\varphi_n)\big)\end{aligned} \tag{41}$$

Eqs. (38) and (41) reveal that the second-order irregular waves are the resultant of the summation of the different interactions between pairs of frequencies [23]. Using these equations to generate a nonlinear irregular wave will lead to dealing with a very complicated nonlinear problem. Therefore, some simplifications have been proposed for this complexity. Agarwal and Manuel [23] showed that changing the double summation in Eqs. (38) and (41) into a single summation can simplify dealing with these equations. Their proposed method takes the benefits of the Inverse Fast Fourier transform. Wang [18,24] also proposed a linearized method by setting the wave surface elevation as a function of a stationary Gaussian process. The present paper defines irregular nonlinear waves based on the Stokes second-order wave theory [22]. Therefore, the wave surface elevation and horizontal particle velocity based on this theory are

$$\eta(t) = \sum_{m=1}^{N} \frac{\mathrm{H_m}}{2}\cos(\omega_m\, t + \varphi_m) + \frac{\pi H_m}{8\,\lambda_m}\frac{\cosh kd}{\sinh^3 kd}[2 + \cosh 2kd\,]\cos(2\,\omega_m t + \varphi_m) \tag{42}$$

And

$$\begin{aligned}u(z,t) &= \sum_{m=1}^{N} \mathrm{u_m}(z,t) \\ &= \sum_{m=1}^{N} f_{1\mathrm{m}}\cosh(k_m z)\cos(\omega_m t + \varphi_m) + f_{2\mathrm{m}}\cosh(2k_m z)\cos\,(2\omega_m t + 2\varphi_m)\end{aligned} \tag{43}$$

Where

$$f_{1\mathrm{m}} = \frac{\omega_m H_m}{2\sinh(k_m d)} \tag{44}$$

$$f_{2\mathrm{m}} = \frac{3}{16} \frac{\omega_m k_m H_m^2}{\sinh^4(k_m d)} \tag{45}$$

H_m is the wave amplitude which can be obtained from the wave spectrum as

$$H_m = \sqrt{2\, S(\omega_m) \Delta\omega_m} \tag{46}$$

Substituting Eq. (43) into Eq. (7), it results in

$$Q(z,t) = \sum_{m=1}^{N} Q_m(z,t) = \sum_{m=1}^{N} F_{1\mathrm{m}}(z,t) + D_m(z,t)\, F_{2\mathrm{m}}(z,t) \tag{47}$$

Where

$$F_{1\mathrm{m}}(z,t) = -\rho_w C_M A \omega_m f_{2\mathrm{m}} \cosh(2k_m z)\, \big(f_m(z)\sin(\omega_m t) + 2\sin(2\omega_m t)\big) \tag{48}$$

$$F_{2\mathrm{m}}(z,t) = \frac{1}{2}\rho_w C_D D f_{2\mathrm{m}}^2 \cosh^2(2k_m z)\, \big(f_m(z)\cos(\omega_m t) + \cos(2\omega_m t)\big)^2 \tag{49}$$

$$D_m(z,t) = \begin{cases} +1, & u_m(z,t) > 0 \\ -1, & u_m(z,t) < 0 \end{cases} \tag{50}$$

Substituting Eq. (47) into Eq. (28) and solving will result in the temporal part of the response, $T(t)$. Therefore, the response is achieved in the form of Eq. (27). For the final step of finding the response, it can be said that

Step 4: Solving Eq. (28) can also be performed for every $Q_m(z,t)$ and the total response can be found by using the superposition principle as

$$\mathrm{x}(z,t) = \sum_{\mathrm{m}=1}^{N} \sum_{\mathrm{n}=1}^{\infty} X_n(z)\, T_m(t) \tag{51}$$

Where

$$\ddot{T}_m(t) + \omega_n^2 \mathrm{T_m}(t) = \frac{1}{EI_M} \int_0^d Q_m(z,t) X_n(z) dz \tag{52}$$

3. A numerical example

To present an example of the proposed method, the DTU 10 MW offshore wind turbine has been selected for the case study introduced by Bak et al. [25]. The foundation and soil properties are also selected from a study conducted by Alkhoury et al. [26] for the same OWT. The properties required for calculating the response based on the proposed method are presented in Table 2.

Table 2) The properties of the DTU 10 MW OWT for the numerical example [25,26]

Structural properties	**Symbol**	**Value**	**Support Stiffness**	**Symbol**	**Value**
Tower length (m)	L_{Tow}	119	Lateral stiffness (GN/m)	K_L	2.48
Tower average diameter (m)	D_{Tow}	6.9	Cross stiffness (GN)	K_{LR}	-20.7
Tower average thickness (m)	t_{Tow}	0.0295	Rotational stiffness (GN.m)	K_R	412
Tower Young's modulus (GPa)	E_{Tow}	210			
Nacelle-Rotor assembly mass (kg)	M_n	676723	**Hydrodynamic loading properties**	**Symbol**	**Value**
Nacelle-Rotor assembly rotational inertia (kg.m2)	J_p	1.7 x 10^8	Water depth (m)	d	25
Platform level from mudline (m)	L_{Plat}	35	Drag coefficient	C_D	0.65
Monopile average diameter (m)	D_{Mon}	8.3	Added mass coefficient	C_A	1
Monopile average thickness (m)	t_{Mon}	0.09	Inertia coefficient	C_M	2
Monopile Young's modulus (GPa)	E_{Mon}	210	Sea water density (kg/m3)	ρ_w	1025
Material Density (kg/m3)	ρ_s	8500			

The natural frequencies of the system should be calculated in the first step. By incorporating the data in Table 2 into the procedure described in section 2.2, the natural frequencies for the first six modes are calculated. The resulting data is presented in Table 3.

Table 3) The natural frequencies of the system

Mode Number	$f_n\ (Hz)$
1	0.1731
2	1.2097
3	2.3000
4	4.0893
5	7.5036
6	11.5126

For verification, the first natural frequency calculated here is compared with the results of a study conducted by Alkhoury et al. [26] for the same DUT 10 MW OWT. They created a full 3D model including all the details of this turbine by using a commercial finite element software program, Abaqus/Standard. Their model is created by the shell elements for the tower structure, including the diameter variation, and solid elements for monopile supporting the tower and its attached components. They also modeled soil inside and outside the monopile to achieve a full detailed model. Also, three models were created, simplifying the modeling of the nacelle-rotor assembly by its mass and rotational mass in "Model 1", changing model 1 by using tapered beam elements instead of shell elements for modeling the tower structure in "Model 2", and simplifying the tower of model 2 with beam elements of constant diameter and thickness in "Model 3". The monopile and the soil surrounding it are modeled the same as the full 3D model for the comparison establishment. The model presented in the present paper is similar to Model 3. The only difference is the simulation of the soil-structure interaction where coupled springs are used in the present work, while a 3D FE-based model entirely simulates it in Model 3. Therefore, the results can be compared, and the degree of accuracy with respect to the full detailed FE model can be estimated. Not that the values of the coupled springs in Table 2 are also obtained by Alkhoury et al. [26] calculated from the full 3D finite element model. Table 4 represents the values of the first natural frequency calculated by Alkhoury et al. [26] and the proposed method. The comparison reveals reasonable agreement even though the foundation is simulated differently. This table also reveals that the simplification made for modeling the tower by a constant diameter underestimates the 1st natural frequency by 13.8% while Alkhoury et al. [26] reported 11%. The differences between the present paper's calculation and their work are due to differences in soil-structure interaction modeling. The natural mode shapes are calculated by the procedure described in section 2.2 and shown in Figure 2. They should also be normalized to fit into Eq. (26).

Table 4) Comparison of the first natural frequency of the system with the FE model

	f_n (Hz)		deviation (%)
	Alkhoury et al. [26]	Proposed model	
Full 3D	0.201		
Model 1	0.206		
Model 2	0.206		
Model 3	0.178	0.173	-2.809

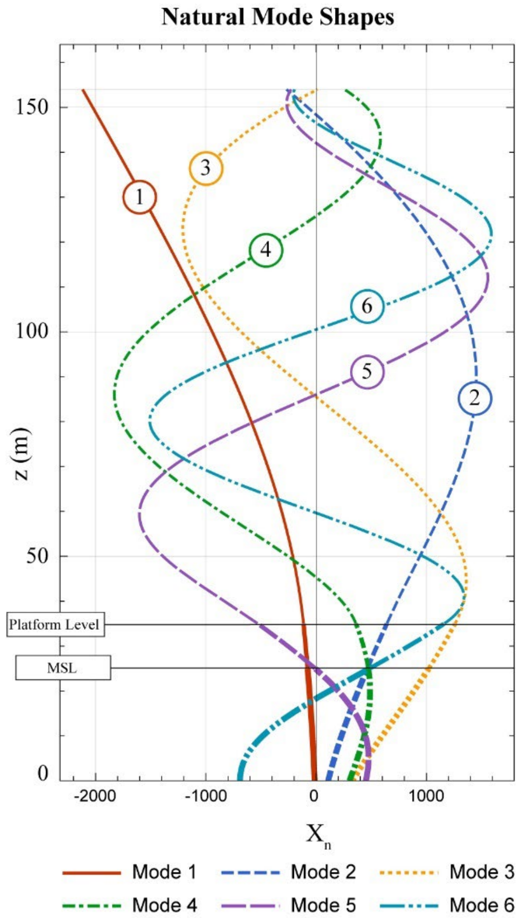

Figure 2) The normalized mode shapes

In this paper, the widely used JANSWAP spectrum [27], which is defined as

$$S(\omega) = (1 - 0.287 \ln \gamma) \frac{5}{6} H_s^2 \, \omega_p^2 \, \omega^{-5} \, \gamma^a \exp\left(-\beta \frac{\omega_p^4}{\omega^4}\right) \tag{53}$$

Where

$$a = \exp\left(-\frac{\left(\omega - \omega_p\right)^2}{2\, \omega_p \, \sigma^2}\right) \tag{54}$$

$$\sigma = \begin{cases} 0.07 & \omega \le \omega_p \\ 0.09 & \omega > \omega_p \end{cases} \tag{55}$$

$$\beta = \frac{5}{4}, \gamma = 3.3 \tag{56}$$

In the above equations, $\omega_p = \frac{2\pi}{T_p}$, T_p, ω , and H_s are defined as the wave peak frequency, wave peak period, wave frequency, and wave significant height, respectively. In the present paper, $H_s = 2.2\, m$ and $T_p = 15\, sec$ are selected as the normal sea state. The wave spectrum calculated based on Eq. (53) and the corresponding wave surface elevation obtained by Eq. (42) are shown in Figure 3 and Figure 4-a, respectively. The response of the system is also calculated by using the proposed method as a function by solving Eq. (28) analytically for every $Q_m(z,t)$ and then summing up the corresponding responses using the superposition principle to achieve the total response. The stress history of the monopile can also be calculated by taking the second derivative of the response function. Therefore, the maximum stress at every point of the monopile can be obtained as a function that can generate data required for fatigue life estimation. The response and stress history (including the stress due to the gravity load) calculated for this paper are shown in Figures 4-b & c, respectively.

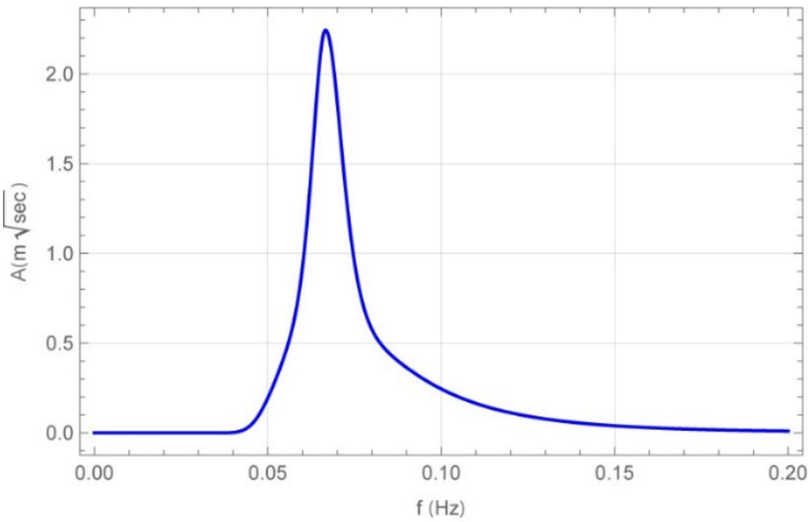

Figure 3) The wave spectrum, $H_s = 2.2\, m$ and $T_p = 15\, sec$

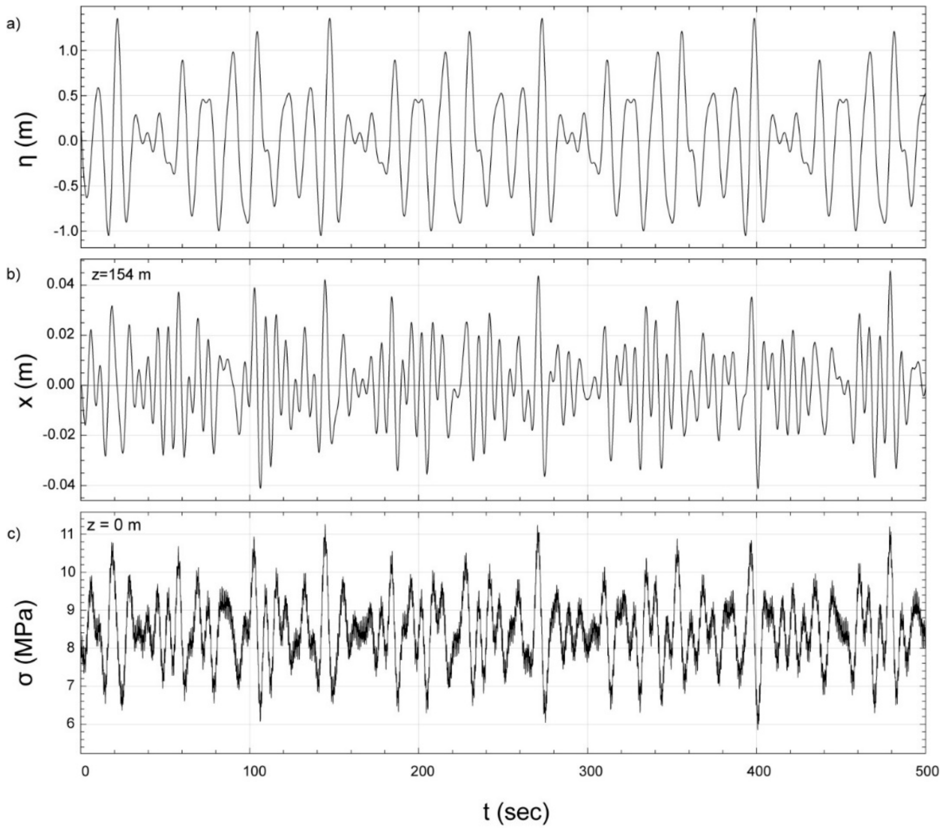

Figure 4) Time series of a) the wave surface elevation, b) the response at the nacelle level, and c) the stress at the mudline, corresponding to the nonlinear irregular waves of $H_s = 2.2\ m$ and $T_p = 15\ sec$

4. Conclusion

This paper develops the response of offshore monopile wind turbines under irregular second-order waves as a function. The structure is divided into three parts to simulate the added mass and geometrical variation. Thus, three different equations of motion were derived for the tower, the monopile above water and the monopile underwater. A series of boundary conditions are implemented at four different levels: the nacelle level, which includes the mass and rotational moment of inertia of the nacelle-rotor assembly, the platform level, which accommodates geometrical differences, the sea level, which separates the monopiles above and below water, and finally, the sea bed level, which incorporates soil-structure interaction. Due to its flexibility in handling complex external forces, the method chosen to solve partial differential equations of motion expands the response by natural modes. Therefore, the response can be obtained as a function that can be used to calculate the stress function at each point of the structure. It is, therefore, possible to generate the stress history required for the analysis of the fatigue life of these structures.

Utilizing the developed process has the advantage of being cost-effective in providing the response and stress history. Additionally, its analytical nature ensures its accuracy. The accuracy of the developed process is highly dependent on the simplifications made in the formulation of equations of motion and boundary conditions.

5. References

[1] Aeran A, Vantadori S, Carpinteri A, Siriwardane SC, Scorza D. Novel non-linear relationship to evaluate the critical plane orientation. Int J Fatigue 2019;124. https://doi.org/10.1016/j.ijfatigue.2019.02.012.

[2] Ivan Komusanac. Repowering analysis. 2021.

[3] Pavlou D. A deterministic algorithm for nonlinear, fatigue-based structural health monitoring. Comput Civ Infrastruct Eng 2022;37. https://doi.org/10.1111/mice.12783.

[4] Amezquita-Sanchez JP, Park HS, Adeli H. A novel methodology for modal parameters identification of large smart structures using MUSIC, empirical wavelet transform, and Hilbert transform. Eng Struct 2017;147:148–59.

[5] Amezquita-Sanchez, Juan P., Adeli H. Feature extraction and classification techniques for health monitoring of structures citation. Sci Iran 2015;22:1931–40.

[6] Martinez-Luengo M, Shafiee M, Kolios A. Data management for structural integrity assessment of offshore wind turbine support structures: data cleansing and missing data imputation. Ocean Eng 2019;173:867–83.

[7] Pavlou DG. Essentials of the Finite Element Method: For Mechanical and Structural Engineers. 2015. https://doi.org/10.1016/C2014-0-03143-7.

[8] Rao SS. Vibration of continuous systems. 2019. https://doi.org/10.1002/9781119424284.

[9] Pavlou DG. Soil–Structure–Wave Interaction of Gravity-Based Offshore Wind Turbines: An Analytical Model. J Offshore Mech Arct Eng 2021;143. https://doi.org/10.1115/1.4048997.

[10] Bazeos N, Hatzigeorgiou GD, Hondros ID, Karamaneas H, Karabalis DL, Beskos DE. Static, seismic and stability analyses of a prototype wind turbine steel tower. Eng Struct 2002;24:1015–25. https://doi.org/10.1016/S0141-0296(02)00021-4.

[11] Murtagh PJ, Basu B, Broderick BM. Along-wind response of a wind turbine tower with blade coupling subjected to rotationally sampled wind loading. Eng Struct 2005;27:1209–19. https://doi.org/10.1016/j.engstruct.2005.03.004.

[12] Lavassas I, Nikolaidis G, Zervas P, Efthimiou E, Doudoumis IN, Baniotopoulos CC. Analysis and design of the prototype of a steel 1-MW wind turbine tower. Eng Struct 2003;25:1097–106. https://doi.org/10.1016/s0141-0296(03)00059-2.

[13] Banerjee A, Chakraborty T, Matsagar V, Achmus M. Dynamic analysis of an offshore wind turbine under random wind and wave excitation with soil-structure interaction and blade tower coupling. Soil Dyn Earthq Eng 2019;125. https://doi.org/10.1016/j.soildyn.2019.05.038.

[14] Alkhoury P, Soubra A-H, Rey V, Aït-Ahmed M. Dynamic analysis of a monopile-supported offshore wind turbine considering the soil-foundation-structure interaction. Soil Dyn Earthq Eng 2022;158:107281. https://doi.org/10.1016/J.SOILDYN.2022.107281.

[15] Wang J, Qin D, Lim TC. Dynamic analysis of horizontal axis wind turbine by thin-walled beam theory. J Sound Vib 2010;329:3565–86. https://doi.org/10.1016/j.jsv.2010.03.011.

[16] Velarde J, Bachynski EE. Design and fatigue analysis of monopile foundations to support the DTU 10 MW offshore wind turbine. Energy Procedia 2017;137:3–13. https://doi.org/10.1016/J.EGYPRO.2017.10.330.

[17] Natarajan A. Influence of second-order random wave kinematics on the design loads of offshore wind turbine support structures. Renew Energy 2014;68:829–41. https://doi.org/10.1016/j.renene.2014.02.052.

[18] Wang Y. Bottom effects on the tower base shear forces and bending moments of a shallow water offshore wind turbine. Mar Struct 2020;70. https://doi.org/10.1016/j.marstruc.2019.102705.

[19] Morison JR, Johnson JW, Schaaf SA. The Force Exerted by Surface Waves on Piles. J Pet Technol 1950;2:149–54. https://doi.org/10.2118/950149-g.

[20] Meirovitch L. Analytical Methods in Vibrations. Macmillan; 1967.

[21] Graff KF. Wave Motion in Elastic Solids. Dover Publications; 2012.

[22] Veritas DN. Environmental conditions and environmental loads. Dnv 2010:9–123.

[23] Agarwal P, Manuel L. Incorporating irregular nonlinear waves in coupled simulation and reliability studies of offshore wind turbines. Appl Ocean Res 2011;33:215–27. https://doi.org/10.1016/J.APOR.2011.02.001.

[24] Wang Y. Efficient prediction of wave energy converters power output considering bottom effects. Ocean Eng 2019;181. https://doi.org/10.1016/j.oceaneng.2019.03.066.

[25] Bak C, Zahle F, Bitsche R, Kim T, Yde A, Henriksen LC, et al. Description of the DTU 10 MW reference wind turbine. 2013.

[26] Alkhoury P, Soubra AH, Rey V, Aït-Ahmed M. A full three-dimensional model for the estimation of the natural frequencies of an offshore wind turbine in sand. Wind Energy 2021;24:699–719. https://doi.org/10.1002/we.2598.

[27] Hasselmann K, Barnett TP, Bouws E, Carlson H, Cartwright DE, Eake K, et al. Measurements of wind-wave growth and swell decay during the joint North Sea wave project (JONSWAP). 1973.